

Gamma ray burst distances and the timescape cosmology

Peter R. Smale^{*}

Department of Physics & Astronomy, University of Canterbury, Private Bag 4800, Christchurch 8140, New Zealand

10 December 2018

ABSTRACT

Gamma ray bursts can potentially be used as distance indicators, providing the possibility of extending the Hubble diagram to redshifts ~ 7 . Here we follow the analysis of Schaefer (2007), with the aim of distinguishing the timescape cosmological model from the Λ CDM model by means of the additional leverage provided by GRBs in the range $2 \lesssim z \lesssim 7$. We find that the timescape model fits the GRB sample slightly better than the Λ CDM model, but that the systematic uncertainties are still too little understood to distinguish the models.

Key words: cosmology: cosmological parameters — cosmology: observations — cosmology: theory

1 INTRODUCTION

The timescape (TS) model is an inhomogeneous cosmological model that explains the apparently accelerated cosmic expansion first observed in the supernova luminosity distances as an artifact of gradients in gravitational energy between gravitationally bound systems and the intervening negatively curved voids. In the dynamical spacetime of general relativity, this leads to a variance in the calibration of the clock rates of ideal observers who fit average smoothed-out geometries to the underlying inhomogeneous matter distribution. The TS model agrees closely with the Λ CDM model over the range of scales probed by the supernova data (Leith et al. 2008), with certain qualifications: parameter values obtained by minimizing χ^2 fits to the TS Hubble curve depend significantly on the process used to reduce the SN Ia light curves (Smale & Wiltshire 2011).

The current state of knowledge of systematic uncertainties in the SN Ia data precludes discrimination between the TS and Λ CDM models using SNe Ia (Smale & Wiltshire 2011). In fact, calculation of the effective comoving distance $H_0 D(z)$ shows that in the redshift range probed by SNe Ia there is little to distinguish between the TS model with the best-fit value for the present void fraction $f_{v0} = 0.762$ from the Gold dataset of Riess et al. (2007). Wiltshire (2009) has noted that over different redshift ranges $H_0 D(z)$ for the TS model closely approximates $H_0 D(z)$ for spatially flat Λ CDM models with different values of Ω_{m0} and $\Omega_{\Lambda 0}$. It is thus seen to interpolate between different Λ CDM models as the redshift is varied (see Fig. 1). Fig. 1 shows that between $z \simeq 2$ and $z \simeq 6$, the TS $H_0 D(z)$ crosses from coinciding closely with the best fit line from the SNe Ia only to that predicted

by the best fit to WMAP, BAO and the SNe Ia. In principle, Gamma Ray Bursts (GRBs), which probe this redshift range, could distinguish the TS and Λ CDM models in this redshift range, although their use as distance indicators is far from established.

This paper will establish that the TS model is also supported by the current GRB data (Schaefer 2007), but that, as one might expect from the SNe Ia results, the uncertainties in the data are as yet too large to distinguish the models in the redshift range $2 < z < 6$.

The paper is organized as follows. Section 2 explains the method of “standardizing” the GRBs for their use as distance indicators, and gives a brief derivation of the TS luminosity distance. Section 3 describes the results, before a discussion and conclusion are presented in Section 4.

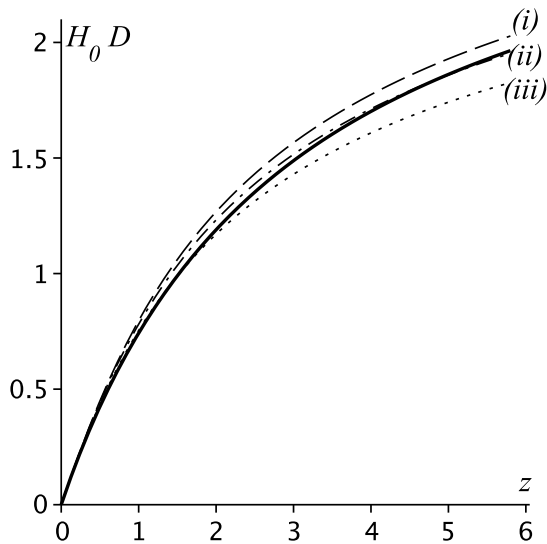
2 BACKGROUND

2.1 The timescape model

In keeping with current observations that the large-scale cosmic structure consists of voids of average diameter $\sim 30 h^{-1}$ Mpc (Hoyle & Vogeley 2004; Pan et al. 2011) separated and threaded by walls and filaments containing clusters of galaxies, the timescape model is based on a differentiation of the Universe into gravitationally bound spatially flat wall regions and negatively curved voids. There is a consequent small backreaction ($\leq 5\%$ as a normalized energy density) which nevertheless leads to significant cosmological effects over cosmological timescales (Wiltshire 2007a). At late epochs the construction of a single smoothed-out geometry becomes problematic when the underlying geometry varies. The TS model is based on the assumption that different equivalent descriptions of a smoothed-out average

^{*} E-mail: peter.smale@pg.canterbury.ac.nz

Figure 1. Effective comoving distance as a function of redshift for various spatially flat models (dotted lines) and for the TS model with $f_{v0} = 0.762$ (solid line). Parameter values for the dotted lines are (i) $\Omega_m = 0.249$ (best-fit to WMAP only); (ii) $\Omega_m = 0.279$ (joint best-fit to WMAP, BAO and SNe Ia); (iii) $\Omega_m = 0.34$ (best-fit to Riess et al. (2007) SNe Ia only). After Wiltshire (2009).



geometry can be given, but these descriptions will vary between canonical observers who each assume that the average geometry has the same spatial curvature as the locally determined geometry. Differences in the calibration of rulers and clocks grow cumulatively as the variance in spatial geometry grows, and these must be taken into account when reconstructing the expansion history of the universe from information on null geodesics.

As observers in galaxies, our local average geometry, assumed to be spatially flat with scale factor a_w , is given by

$$ds_{fi}^2 = -d\tau^2 + a_w^2(\tau)[d\eta_w^2 + \eta_w^2 d\Omega^2]. \quad (1)$$

Finite infinity (Ellis 1984), denoted by fi , demarcates the boundary between gravitationally bound and unbound systems (Wiltshire 2007a). A similar expression defines the negatively curved geometry at the centre of a void, with an appropriate void time parameter τ_v and scale factor a_v .

The volume averaged scale factor

$$\bar{a}^3 = f_{v_i} a_v^3 + (1 - f_{v_i}) a_w^3, \quad (2)$$

where $f_{v_i} \ll 1$ is the initial void fraction, evolves according to an averaging of the Einstein equations for an inhomogeneous dust cosmology due to Buchert (2000). The corresponding averaged geometry, in terms of the proper time t at a volume average position in freely expanding space, has the form

$$ds^2 = -dt^2 + \bar{a}^2(t) d\bar{\eta}^2 + A(\bar{\eta}, t) d\Omega^2, \quad (3)$$

where the area function A is defined by an average over the particle horizon volume (Wiltshire 2007a). The local time in a wall is related to t by the phenomenological lapse parameter $\bar{\gamma} = \frac{dt}{d\tau}$.

A single geometry that relates metrics (1) and (3) is constructed by matching the radial null geodesics of wall and volume average geometries sharing a common centre (Wiltshire (2007a), § 5.2). Along the radial null geodesics, the line elements of the two geometries are simply related by a conformal factor. Once the metric is extended to cosmological scales, instead of (3) wall observers describe the large-scale universe by the effective metric

$$ds^2 = -d\tau^2 + \frac{\bar{a}^2}{\bar{\gamma}^2} [d\bar{\eta}^2 + r_w^2(\bar{\eta}, t) d\Omega^2], \quad (4)$$

where $r_w \equiv \bar{\gamma}(1 - f_v)^{1/3}(1 - f_{v_i})^{-1/3} \eta_w(\bar{\eta}, t)$. Metric (4) is the “dressed” geometry that arises when we attempt to reconcile our position as observer within a finite infinity region with observations of objects at cosmological distances. In general, observers (localised within finite infinity regions) cannot assume that their measurements of cosmological parameters correspond to the global average values. However, due to the existence of a scale of statistical homogeneity, the values of locally measured cosmological parameters should converge towards their global average values as the averaging volume increases.

Volume average (“bare”) parameters, referred to metric (3), differ from dressed parameters. The dressed matter density is $\Omega_m = \bar{\gamma}^3 \bar{\Omega}_{m0}$, and the Hubble parameter of metric (4) is related to the bare Hubble parameter according to

$$H = \bar{\gamma} \bar{H} - \frac{d}{dt} \bar{\gamma}. \quad (5)$$

It is a feature of the TS model that the variance of parameters calculated from observations of nearby objects (on scales $\lesssim 100 h^{-1}$ Mpc) will be relatively large because such objects lie within the scale of statistical homogeneity. Since the volume of space is dominated by voids — of typical diameter $\sim 30 h^{-1}$ Mpc — which appear to expand faster than the walls, observers in a typical galaxy looking on a typical line of sight through local voids will infer that their local universe is expanding faster than the global average. Eventually a typical line of sight will intersect a sufficient number of walls as well as voids to approach the global average, which does not change by sampling on ever larger scales. The transition scale from large to small variance in the expansion must be larger than the diameter of the dominant voids, and is referred to as the *scale of statistical homogeneity*. It is expected to be comparable to the BAO scale, $\sim 100 h^{-1}$ Mpc (Wiltshire 2008). Thus any observer in a galaxy will typically see a “Hubble bubble” on scales $\lesssim 100 h^{-1}$ Mpc.

In terms of volume average time, t , the luminosity distance for wall observers is (Wiltshire 2007b)

$$d_L = \bar{a}_0(1 + z)r_w. \quad (6)$$

The Buchert equations have an exact general solution which admits a particular late-time attractor solution, to which the general solution converges to within 1% by redshift $z \sim 37$ (Wiltshire 2007b). For this tracker solution, eq. (6)

becomes (Wiltshire 2009)

$$\begin{aligned} \bar{H}_0 d_L &= (1+z)^2 (\bar{H}_0 t)^{2/3} \int_t^{t_0} \frac{2\bar{H}_0 dt}{(2+f_v(t'))(\bar{H}_0 t)^{2/3}} \quad (7) \\ &= (1+z)^2 y^2 \times \\ &\quad \left[2y + \frac{b}{6} \ln \left(\frac{(y+b)^2}{y^2 - by + b^2} \right) + \frac{b}{\sqrt{3}} \tan^{-1} \left(\frac{2y-b}{\sqrt{3}b} \right) \right]_y \end{aligned}$$

where $y^3 \equiv \bar{H}_0 t$ and $b^3 \equiv 2(1-f_{v0})(2+f_{v0})/(9f_{v0})$. In Fig. 1, $D = d_L/(1+z)$, and the dressed Hubble constant H_0 , is related to the bare Hubble constant \bar{H}_0 by

$$H_0 = (4f_{v0}^2 + f_{v0} + 4)/[2(2+f_{v0})]\bar{H}_0. \quad (8)$$

The dressed Hubble constant is the one whose value should coincide with that which is conventionally determined on scales greater than the scale of statistical homogeneity, $z \gtrsim 0.033$. Using the ‘‘Gold’’ SN Ia dataset of Riess et al. (2007), Leith et al. (2008) found the dressed Hubble constant to be $H_0 = 61.7^{+1.4}_{-1.3} \text{ km sec}^{-1} \text{ Mpc}^{-1}$, (and the bare Hubble constant $\bar{H}_0 = 48.2 \pm 2.6 \text{ km sec}^{-1} \text{ Mpc}^{-1}$). However, since the supernova data magnitudes depend on an overall normalization determined from the local distance ladder, they cannot be used to determine the Hubble constant alone. Joint estimates of H_0 and f_{v0} which fit both the angular diameter distance of the sound horizon in the CMB anisotropy data and the baryon acoustic oscillation scale in galaxy clustering statistics do provide an independent constraint on the value of H_0 , however, and on this basis Leith et al. (2008) find the range of values of the dressed Hubble constant to be roughly constrained to lie in the interval $57 \lesssim H_0 \lesssim 68 \text{ km sec}^{-1} \text{ Mpc}^{-1}$. This is lower than the $SH_0\text{ES}$ best estimate of Riess et al. (2011) but that survey relies on the calibration of the distance ladder using objects that lie within the scale of statistical homogeneity, and this may involve complicated systematics given that higher values of H_0 are expected below the statistical homogeneity scale. Estimates of H_0 which do not rely on calibration with nearby objects are often somewhat lower. For example, Courbin et al. (2010) find $H_0 = 62^{+6}_{-4} \text{ km sec}^{-1} \text{ Mpc}^{-1}$ using the time delay from strong gravitational lensing of quasars, and Beutler et al. (2011) estimate $H_0 = 67 \pm 3.2 \text{ km sec}^{-1} \text{ Mpc}^{-1}$ using the WMAP sound horizon-calibrated BAO signal in the 6dF galaxy survey. These measurements indicate that a value of H_0 consistent with the TS model is still to be obtained once systematic errors on distance determinations are reduced.

With the tracker solution, the bare densities $\bar{\Omega}_{m0}$ and $\bar{\Omega}_{k0}$ can be written in terms of the present void fraction. In particular, the dressed matter density, measured by wall observers, for which the numerical value is most likely to be similar to that of a FLRW model, will be

$$\Omega_{m0} = \frac{1}{8}(2+f_{v0})^3 \bar{\Omega}_{m0} = \frac{1}{2}(1-f_{v0})(2+f_{v0}) \quad (9)$$

for the tracker solution.

Since there is no nearby GRB sample, there is no GRB calibration of \bar{H}_0 , and we work with relative distances only. The fitting process therefore results in a best-fit value for the single parameter f_{v0} .

2.2 GRB data reduction method

In this paper I will use the sample of 69 GRBs selected by Schaefer (2007) (henceforward S07) as having sufficient light curve data to compute their placement on a Hubble diagram.

GRBs are not standard candles, since their luminosities span several orders of magnitude (whether one assumes collimated or isotropic emission). However, there are ongoing attempts to ‘‘standardize’’ GRBs given their promise for cosmology: they occur at higher redshifts than any established standard candles, and radiation in the gamma band ($\geq 10 \text{ keV}$) is not subject to the same limitations due to dust extinction as the optical band (Ghirlanda, Ghisellini & Firmani 2006). Certain GRB light curve parameters have been found to correlate with each other, offering the possibility of computing a magnitude, much in the same way as the Phillips stretch-luminosity relation is used to reduce scatter in the SN Ia Hubble diagram.

Schaefer (2007) uses four light curve parameters that correlate with the luminosity: (1) the lag time τ_{lag} is the time shift between the hard and the soft light curves; (2) the light curve variability V is the normalized variance of the light curve around a smoothed version of that light curve; (3) the peak energy E_{peak} is the photon energy at which the νF_ν spectrum is brightest; and (4) the minimum rise time τ_{RT} is the shortest time over which the light curve rises by half the peak flux of the pulse. A fifth correlation, $E_{\text{peak}} - E_\gamma$, relates the peak energy of the light curve to total photon energy emitted by the burst. This is the tightest of the correlations (Ghirlanda et al. 2004), but it requires measurement of a jet break time by which the measured (isotropic-equivalent) energy can be corrected for the collimation. Along with these luminosity indicators a peak flux P is also measured for a wide range of bandpasses. A bolometric flux (or fluence) can be calculated by extrapolating to high and low energies using the well-known broken power law of Band et al. (1993) for the GRB spectrum and integrating over all energies. This brings consistency to the brightnesses, and given a cosmological model, permits the calculation of an isotropic luminosity

$$L = 4\pi d_L^2 P_{\text{bolo}}. \quad (10)$$

The algorithm goes as follows. The luminosity indicator is the independent variable, and from eq. (10) is obtained the Y -coordinate. A linear fit to the logarithms of these quantities gives an empirical relationship between the luminosity indicator and the luminosity. For this fit, we use the bisector of the two ordinary least squares fits: that of X against Y , and then vice versa (Isobe et al. 1990). We can then use this relationship to calculate a theoretical luminosity curve for each indicator, based on the luminosity distance obtained from eq. (10). In cases where a jet break has been measured, E_{peak} is related to the collimation-corrected energy E_γ , by

$$E_\gamma = 4\pi d_L^2 S_{\text{bolo}} (1 - \cos \theta_{\text{jet}}) (1+z)^{-1}, \quad (11)$$

for jet opening angle θ_{jet} and bolometric fluence S_{bolo} . The uncertainties in the Y -axis quantities $\log L$ and $\log E_\gamma$ are obtained from the uncertainties in the X -axis quantities in the standard way. Because the physics of the GRB explosions is not completely understood, the correlations contain some scatter over and above the measurement noise. To ac-

count for this, an additional intrinsic uncertainty is estimated such that the reduced χ^2 of the indicator-luminosity calibration curve is unity. The best-fit lines for these relations are given along with their uncertainties in Appendix A.

From each calculated L or E_γ we then recalculate a luminosity distance via (10) or (11), from which we obtain a distance modulus in the standard way: $\mu = 5 \log d_L - 25$ for d_L in Mpc. The propagated uncertainties are (Schaefer 2007)

$$\sigma_\mu^2 = (2.5\sigma_{\log L})^2 + \left(\frac{1.086\sigma_{P_{\text{bolo}}}}{P_{\text{bolo}}}\right)^2, \quad (12)$$

if the bolometric flux P_{bolo} is used, or, if the bolometric fluence is used,

$$\sigma_\mu^2 = (2.5\sigma_{\log E_\gamma})^2 + \left(\frac{1.086\sigma_{S_{\text{bolo}}}}{S_{\text{bolo}}}\right)^2 + \left(\frac{1.086\sigma_{F_{\text{beam}}}}{F_{\text{beam}}}\right)^2, \quad (13)$$

where the beam factor $F_{\text{beam}} \equiv (1 - \cos \theta_{\text{jet}})$ is calculated from the jet break time t_{jet} .

Finally, we take a weighted average of all the five different distance moduli:

$$\mu = \frac{\sum_i \mu_i / \sigma_{\mu_i}^2}{\sum_i \sigma_{\mu_i}^{-2}}, \quad (14)$$

with the uncertainty

$$\sigma_\mu = \left(\sum_i \sigma_{\mu_i}^{-2}\right)^{-1/2}. \quad (15)$$

We avoid circularity by performing a simultaneous fit of both the cosmology and the luminosity relations (Ghirlanda et al. 2004; Schaefer 2007)—i.e. the luminosity relations are part of the model. The value of H_0 here is arbitrary, since its variation changes the Hubble line and the luminosity calibration of the data in an identical way, resulting merely in a change in the overall normalization of the Hubble diagram. GRBs do not occur in the local universe, so calibrating the GRB Hubble diagram to a value of H_0 with any accuracy is not possible. This is different to the SN Ia case, in which the calibration of light curve and stretch can be done model-independently with nearby SNe Ia, and then extrapolated to objects at higher redshifts. However, regardless of the normalization, the *shape* of the curve in the Hubble diagram depends solely on $f_{v,0}$. This means that for a range of values of $f_{v,0}$, here between 0.0 and 1.0, we calibrate the luminosity relation and compute the placement of the GRBs on the Hubble diagram, and calculate a corresponding range of χ^2 values. The favoured value for $f_{v,0}$ is that for which the χ^2 is minimized.

3 RESULTS

We show the results of the linear regressions in figures 2–6 in black. The intercept a and slope b of the TS model calibration line are shown in each figure. For comparison, the Λ CDM-calibrated data points (for a flat Friedmann model with $\Omega_m = 0.27$ and $w = -1$, as calculated in S07) are shown in grey.

The timescape model produces calibrations that are within 1σ of the Λ CDM model in each case. In fact, the TS model regression parameters match those of the concordance model more closely than regression parameters calculated from the variable dark energy equation of state cosmology

Figure 2. Power law relation between lag time τ_{lag} , corrected to the GRB rest frame, and isotropic luminosity, for 38 GRBs. The 1σ measurement uncertainties are used for the error bars. The Λ CDM fit as calculated in Schaefer (2007) is shown in grey. The intercept a and the slope b for the TS calibration are shown on the plot, and the equation of the best-fit line and the expected uncertainty in the luminosity so calculated is given in Appendix A(i).

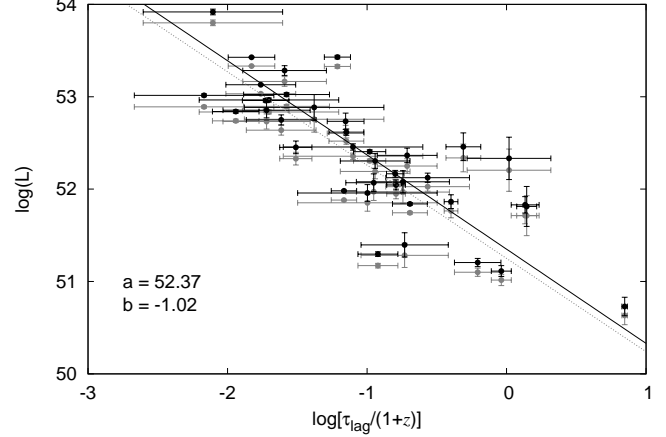
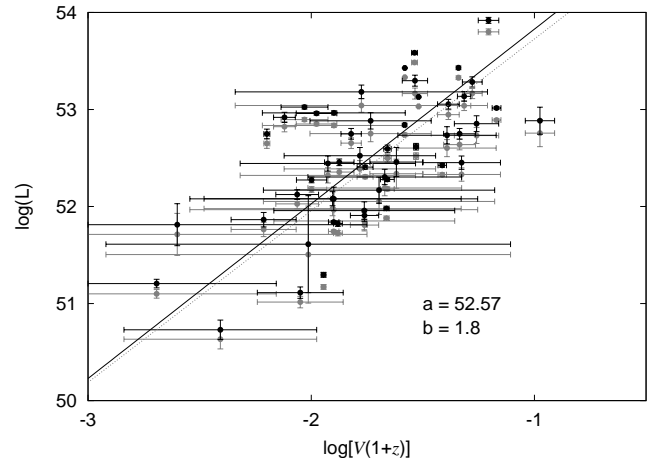


Figure 3. Bisector fit of the Variability-Luminosity relation for 51 GRBs. Larger measurement uncertainties in this relation mean it carries less weight in the final luminosity average. The TS intercept a and the slope b are shown, and the equation of the best-fit line and the expected uncertainty in the luminosity so calculated are given in Appendix A(ii).



of Riess et al. (2004) ($w_0 = -1.31$, $w' = 1.48$), computed in S07 to assess the dependence of the calibration on the input cosmology.

The resulting Hubble diagram for the TS model is shown in fig. 7. In the Λ CDM case, with the “concordance” value $\Omega_m = 0.27$, we obtain a reduced χ^2 of 1.05 as in S07. The parameter values that minimize the HD χ^2 are $\Omega_m = 0.21^{+0.22}_{-0.11}$ for the Λ CDM model¹, shown in grey, and

¹ This coincides within a standard deviation with $\Omega_m =$

Figure 4. Bisector fit of GRB isotropic luminosity to the peak energy E_{peak} , corrected to the rest frame of the GRB. $N = 64$. The TS intercept a and the slope b , and the equation of the best-fit line and the expected uncertainty in the luminosity so calculated are given in Appendix A(iii).

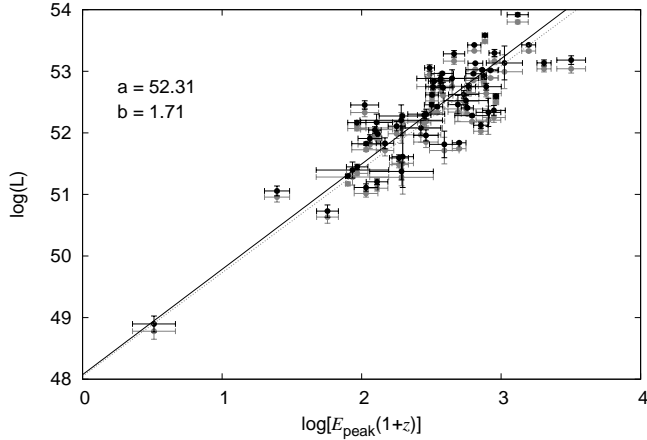
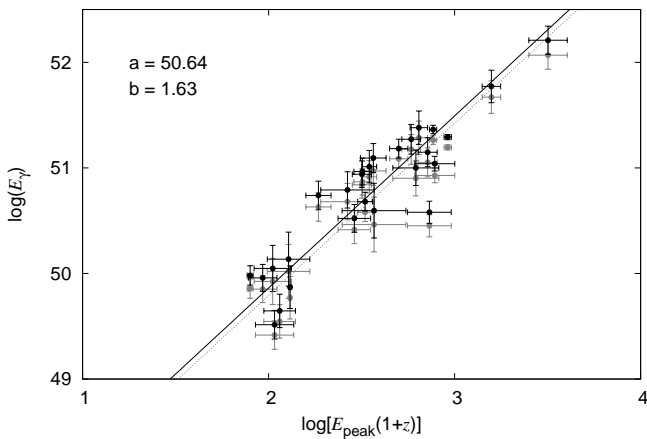


Figure 5. $E_{\text{peak}} - E_{\gamma}$ relation for 27 GRBs. This is the tightest of the five power relations but there are fewer data points, since calculation of E_{γ} requires identification and measurement of a jet break. The TS intercept a and the slope b are shown on the plot, and the equation of the best-fit line and the expected uncertainty in the E_{γ} so calculated are given in Appendix A(iv).



$f_{v0} = 0.84^{+0.14}_{-0.21}$ for the timescape model, for which the reduced χ^2 was 1.04 for 68 dof, shown in black. This present void fraction corresponds to a matter density as measured by wall observers via eq. (9) of $\Omega_m = 0.23^{+0.25}_{-0.20}$. However, note that there is no *a priori* reason why the Λ CDM and TS values for Ω_m should coincide, since the role of this parameter in each theory is different.

The TS model fits the GRB Hubble diagram slightly better (lower χ^2) than the Λ CDM model. The correspond-

$0.39^{+0.12}_{-0.08}$ found in S07, which was found by marginalizing over the slopes and intercepts of the luminosity relations.

Figure 6. Minimum rise time-Luminosity relation for 62 GRBs. The TS intercept a and the slope b are shown, and the equation of the best-fit line and the expected uncertainty in the luminosity so calculated are given in Appendix A(v).

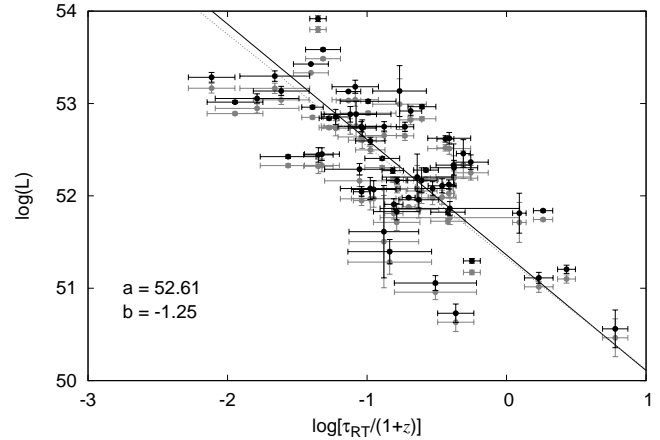
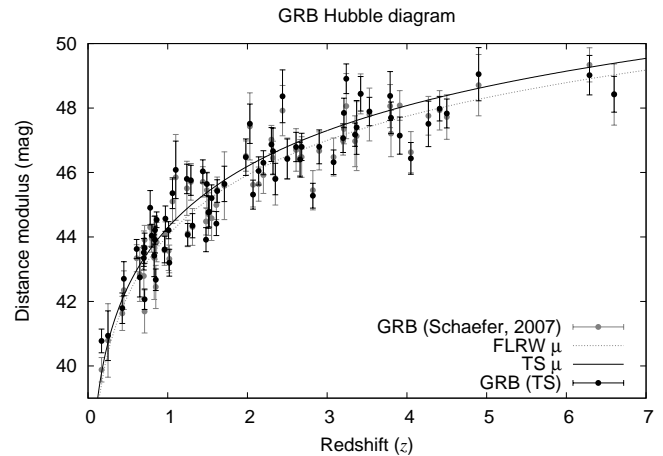


Figure 7. Hubble diagram for the 69 GRBs of S07. The Λ CDM diagram is shown in grey, and the TS diagram is shown in black.



ing Bayes factor $\ln B = 0.18$ indicates Bayesian evidence in favour of the timescape model that is “not worth more than a bare mention” according to the Jeffreys scale (Kass & Raftery 1995). This is apparent, since the competing predictions of the models lie well within the range spanned by the measurement errors, let alone the systematics, so it can only be concluded that GRB cosmology is not yet precise enough to distinguish between these models.

By contrast, preliminary investigations by Schaefer (2008) indicate that certain modified gravity models and particular exotic forms of dark energy (the Chaplygin gas) provide much poorer fits to the GRB data than the standard Λ CDM model. Amongst the alternatives to the Λ CDM model, the TS model therefore enjoys a degree of phenomenological success which is hard to replicate in a number of other scenarios.

4 CONCLUSION

Some issues with the use of GRBs as standard candles for constraining cosmological parameters are discussed by Ghirlanda, Ghisellini & Firmani (2006), Ghirlanda (2009), and Petrosian et al. (2009). In particular, the correlations between the isotropic luminosities and the luminosity indicators are weak in a χ^2 sense—physical factors unaccounted for are producing large scatter. Strictly speaking, the $E_{\text{peak}} - E_\gamma$ correlation is the only relationship with a sufficiently low reduced χ^2 to admit cosmological parameter estimation, albeit with the caveat that the measurement of the jet break time assumes a particular fireball model (Ghirlanda 2009). Petrosian et al. (2009) point out that the luminosity correlations are statistical in nature, rather than being, as they should ideally, one-to-one relations between uncorrelated quantities. This meant, for example, that the comparatively tight $E_{\text{peak}} - E_\gamma$ correlation found by Ghirlanda et al. (2004) actually weakened with the introduction of more data points.

Systematic uncertainties such as dust extinction and evolution constitute considerable limitations to cosmological parameter estimation with SNe Ia. Many of these uncertainties, for example Malmquist bias and gravitational lensing, are considered negligible in the redshift range over which SNe Ia occur. For the redshift range over which GRBs occur, one would expect that Malmquist bias and lensing might cause at least some of the scatter in the GRB Hubble diagram, but these biases are shown in S07 to be negligibly small. Obscuration by dust is not an issue for GRBs (Ghirlanda et al. 2004), but selection and evolution effects can potentially influence the current GRB sample. The well-known “Amati” correlation for long-duration GRBs between isotropic-equivalent radiated energy E_{iso} , describing the intensity of the burst, and the photon energy at which the time-averaged spectrum peaks $E_{\text{p},i}$, although proving to be quite robust (Amati et al. 2008; Amati 2010), has shown evidence of variation with redshift (Li 2007) and susceptibility to detector threshold selection effects (Butler et al. 2007). Petrosian et al. (2009) find evidence for evolution of the GRB peak luminosities, but this should not affect the Hubble diagram, since it is the luminosity relations which should give the right distances for placement on the Hubble diagram.

It can be argued that the kind of relativistic and geometric effects that underlie the luminosity relations should not be greatly affected by evolution or the metallicity of the progenitor (Schaefer 2007). It is conceivable that a better understanding of GRB physics in the future will allow them to be used as “standardizable” candles, and put their utility for cosmological parameter estimation and discrimination between cosmological models on a firmer basis. Ongoing observational programmes such as *Swift* continue to contribute to this aim. We need to know more about the physics of the GRBs, and we need more high-quality measurements of GRB redshifts, light curves and spectra.

In the meantime, however, we can obtain glimpses of the potential applications of standard candles whose range extends into the era of decelerating cosmic expansion. In the present study, the correlations are forced to be a good fit by incorporating the additional “systematic error” term, computed such that it makes the χ^2 of the best-fit correlation equal to one. This term contributes (in quadrature) to

the uncertainty in the log of the isotropic luminosity which propagates through to the Hubble diagram χ^2 via eqs (12) and (13). A single GRB at a redshift of 5 or 6, with better-determined physical characteristics, potentially carries more statistical power than a single SN Ia at $z = 1.7$ because of the Hubble diagram “lever arm”—the Hubble diagram at redshifts $z > 2$ changes with a different cosmological model or cosmological parameters much more than it does at lower redshifts. We obtain results that are not inconsistent with current models, with certain acknowledged caveats. In particular, there is much scope for progress in improving the GRB Hubble diagram, and much to be gained.

ACKNOWLEDGMENTS

I thank David Wiltshire for suggestions and discussions. This work was supported by a University of Canterbury Doctoral Scholarship and the Marsden fund of the Royal Society of New Zealand.

APPENDIX A: TIMESCAPE CALIBRATION CURVE EQUATIONS

The five calibrations in figures 2–6 are based on the bisector of the two ordinary least squares fits (Isobe et al. 1990). For the i th luminosity indicator, the best-fit line has the form $Y_i = a + bX_i$, where $X_i = \log(\text{indicator}) \pm \log(1+z)$, where the sign of the redshift factor depends on the indicator. The five best-fit lines for the TS model (those for which the HD χ^2 is a minimum), their associated uncertainties, and the corresponding Λ CDM values for a and b , are given below.

(i) *Lag time vs. Luminosity:*

For the timescape model:

$$\log L = 52.37 - 1.02 \log \left[\frac{\tau_{\text{lag}}(1+z)^{-1}}{0.1 \text{ s}} \right]; \quad (\text{A1})$$

$$\sigma_{\log L}^2 = \sigma_a^2 + \left\{ \sigma_b \log \left[\frac{\tau_{\text{lag}}(1+z)^{-1}}{0.1 \text{ s}} \right] \right\}^2 + \left(\frac{0.4343b\sigma_{\text{lag}}}{\tau_{\text{lag}}} \right)^2 + \sigma_{\text{lag,sys}}^2, \quad (\text{A2})$$

where $\sigma_a = 0.13$, $\sigma_b = 0.09$, and $\sigma_{\text{lag,sys}}^2 = 0.37$ gives a reduced χ^2 of one. For the Λ CDM calibration, we find $a = 52.30 \pm 0.13$, $b = -1.00 \pm 0.09$ and $\sigma_{\text{lag,sys}}^2 = 0.36$.

(ii) *Variability vs. Luminosity:*

For the timescape model:

$$\log L = 52.57 + 1.80 \log \left[\frac{V(1+z)}{0.02} \right]; \quad (\text{A3})$$

$$\sigma_{\log L}^2 = \sigma_a^2 + \left\{ \sigma_b \log \left[\frac{V(1+z)}{0.02} \right] \right\}^2 + \left(\frac{0.4343b\sigma_V}{V} \right)^2 + \sigma_{V,\text{sys}}^2, \quad (\text{A4})$$

where $\sigma_a = 0.34$, $\sigma_b = 0.20$, and $\sigma_{V,\text{sys}}^2 = 0.35$ gives a reduced χ^2 of one. For the Λ CDM calibration, we find $a = 52.50 \pm 0.34$, $b = 1.77 \pm 0.20$ and $\sigma_{V,\text{sys}}^2 = 0.35$.

(iii) E_{peak} vs. *Luminosity*:

For the timescape model:

$$\log L = 52.31 + 1.71 \log \left[\frac{E_{\text{peak}}(1+z)}{300 \text{ keV}} \right]; \quad (\text{A5})$$

$$\sigma_{\log L}^2 = \sigma_a^2 + \left\{ \sigma_b \log \left[\frac{E_{\text{peak}}(1+z)}{300 \text{ keV}} \right] \right\}^2 + \left(\frac{0.4343b\sigma_{E_{\text{peak}}}}{E_{\text{peak}}} \right)^2 + \sigma_{E_{\text{peak,sys}}}^2, \quad (\text{A6})$$

where $\sigma_a = 0.24$, $\sigma_b = 0.10$, and $\sigma_{E_{\text{peak,sys}}}^2 = 0.34$ gives a reduced χ^2 of one. For the Λ CDM calibration, we find $a = 52.24 \pm 0.24$, $b = 1.69 \pm 0.10$ and $\sigma_{E_{\text{peak,sys}}}^2 = 0.34$.

(iv) E_{peak} vs. E_γ :

For the timescape model:

$$\log E_\gamma = 50.64 + 1.63 \log \left[\frac{E_{\text{peak}}(1+z)}{300 \text{ keV}} \right]; \quad (\text{A7})$$

$$\sigma_{\log E_\gamma}^2 = \sigma_a^2 + \left\{ \sigma_b \log \left[\frac{E_{\text{peak}}(1+z)}{300 \text{ keV}} \right] \right\}^2 + \left(\frac{0.4343b\sigma_{E_{\text{peak}}}}{E_{\text{peak}}} \right)^2 + \sigma_{E_\gamma, \text{sys}}^2, \quad (\text{A8})$$

where $\sigma_a = 0.28$, $\sigma_b = 0.10$, and $\sigma_{E_\gamma, \text{sys}}^2 = 0.17$ gives a reduced χ^2 of one. For the Λ CDM calibration, we find $a = 50.58 \pm 0.28$, $b = 1.62 \pm 0.10$ and $\sigma_{E_\gamma, \text{sys}}^2 = 0.15$.

(v) *Rise time vs. Luminosity*:

For the timescape model:

$$\log L = 52.61 - 1.25 \log \left[\frac{\tau_{\text{RT}}(1+z)^{-1}}{0.1 \text{ s}} \right]; \quad (\text{A9})$$

$$\sigma_{\log L}^2 = \sigma_a^2 + \left\{ \sigma_b \log \left[\frac{\tau_{\text{RT}}(1+z)^{-1}}{0.1 \text{ s}} \right] \right\}^2 + \left(\frac{0.4343b\sigma_{E_{\text{peak}}}}{E_{\text{peak}}} \right)^2 + \sigma_{\tau_{\text{RT,sys}}}^2, \quad (\text{A10})$$

where $\sigma_a = 0.11$, $\sigma_b = 0.11$, and $\sigma_{\tau_{\text{RT,sys}}}^2 = 0.48$ gives a reduced χ^2 of one. For the Λ CDM calibration, we find $a = 52.54 \pm 0.11$, $b = -1.23 \pm 0.11$ and $\sigma_{\tau_{\text{RT,sys}}}^2 = 0.47$.

Ellis, G. F. R., 1984, in Bertotti, B., de Felice, F. & Pascolini, A. (eds), *General Relativity and Gravitation*, (Reidel, Dordrecht) pp. 215–288.

Ellis, G. F. R. & Stoeger, W., 1987, *Class. Quantum Grav.* **4**, 1697.

Freedman, W. L. *et al.*, 2001, *ApJ* **553**, 47.

Ghirlanda, G., Ghisellini, G., Lazzati, C., & Firmani, C., 2004, *ApJ* **613**, L13

Ghirlanda, G., Ghisellini, G., and Firmani, C., 2006, *New J. Phys.* **8**, 123.

Ghirlanda, G., in Antonelli, L. A., Limongi, M., Menci, N., Tornambe, A., Brocato, E., & Raimondo, G. (eds), 2009, *Probing Stellar Populations out to the Distant Universe*, AIP Conference Proceedings **1111**, pp. 579–586.

Hoyle, F. and Vogeley, M. S., 2004, *ApJ* **607**, 751.

Isobe, T., Feigelson, E. D., Akritas, M. G., and Babu, G. J., 1990, *ApJ* **364**, 104.

Kass, R. E. & Raftery, A. E., 1995, *J. Amer. Statistical Assoc.* **90**, 773.

Leith, B. M., Ng, S. C. C. & Wiltshire, D. L., 2008, *ApJ* **672**, L91.

Li, L. X., 2007, *MNRAS* **379**, L55.

Pan, D. C., Vogeley, M. S., Hoyle, F., Choi, Y. Y., & Park, C., 2011, arXiv:1103.4156 [astro-ph.CO].

Perlmutter, S. *et al.*, 1999, *ApJ* **517**, 565.

Petrosian, V., A. Bouvier, A., & Ryde, F., 2009, arXiv:0909.5051 [astro-ph.HE].

Riess, A. G., Press, W. H. & Kirshner, R. P., 1995, *ApJ* **438**, L17.

Riess, A. G. *et al.*, 1998, *AJ* **116**, 1009.

Riess, A. G. *et al.*, 2004, *ApJ* **607**, 665.

Riess, A. G. *et al.*, 2007, *ApJ* **659**, 98.

Riess, A. G. *et al.*, 2011, *ApJ* **730**, 119.

Schaefer, B. E., 2007, *ApJ* **660**, 16.

Schaefer, B. E., 2008, talk at Sixth Huntsville Gamma Ray Symposium, <http://grbhunstableville2008.cspaar.aah.edu/content/Talks/Schaefer.pdf>

Smale, P. R., & Wiltshire, D. L., 2011, *MNRAS* **413**, 367

Wiltshire, D. L., 2007a, *New J. Phys.* **9**, 377.

Wiltshire, D. L., 2007b, *Phys. Rev. Lett.* **99**, 251101.

Wiltshire, D. L., 2008, *Phys. Rev. D* **78**, 084032.

Wiltshire, D. L., 2009, *Phys. Rev. D* **80**, 123512.

REFERENCES

- Amati, L., Guidorzi, C., Frontera, F., Della Valle, M., Finelli, F., Landi, R., Montanari, E., 2008, *MNRAS* **391**, 577.
- Amati, L., 2010, arXiv:1002.2232 [astro-ph.HE].
- Band, D., Matteson, J., Ford, L., Schaefer, B., Palmer, D., Teegarden, B., Cline, T., Briggs, M., Paciesas, W., Pendleton, G., Fishman, G., Kouveliotou, C., Meegan, C., Wilson, R., Lestrade, P., 1993, *ApJ* **413**, 281.
- Beutler, F. *et al.*, 2011, arXiv:1106.3366 [astro-ph.CO].
- Buchert, T., 2000, *Gen. Relativ. Grav.* **32**, 105.
- Butler, N. R., Kocevski, D., Bloom, J. S., Curtis, J. L., 2007, *ApJ* **671**, 656.
- Cardelli, J. A., Clayton, G. C. & Mathis, J. S., 1989, *ApJ* **345**, 245.
- Courbin, F. *et al.*, 2010, arXiv:1009.1473 [astro-ph.CO].